Cell Death & Differentiation (2021) 28:2160–2178
https://doi.org/10.1038/s41418-021-00744-9

Cell Death & Differentiation

ARTICLE

MACF1 promotes osteoblast differentiation by sequestering repressors in cytoplasm

Lifang Hu[1,2,3,4] · Chong Yin[1,2,3,4] · Dong Chen[5,6] · Zixiang Wu[1,2,3,4] · Shujing Liang[1,2,3,4] · Yu Zhang[6] · Zizhan Huang[1,2,3,4] · Shuyu Liu[1,2,3,4] · Xia Xu[1,2,3,4] · Zhihao Chen[1,2,3,4] · Yi Zhang[5,6] · Airong Qian[1,2,3,4]

Received: 6 September 2019 / Revised: 22 January 2021 / Accepted: 28 January 2021 / Published online: 4 March 2021

Abstract

Osteoblast differentiation leading to bone formation requires a coordinated transcriptional program. Osteoblastic cells with low level of microtubule actin crosslinking factor 1 (MACF1) show reduced osteoblast differentiation ability, however, the comprehensive mechanism of MACF1's action remains unexplored. In the current study, we found that MACF1 knockdown suppressed osteoblast differentiation by altering the transcriptome dynamics. We further identified two MACF1-interacted proteins, cyclin-dependent kinase 12 (CDK12) and MYST/Esa1-associated factor 6 (MEAF6), and two MACF1-interacted transcription factors (TFs), transcription factor 12 (TCF12) and E2F transcription factor 6 (E2F6), which repress osteoblast differentiation by altering the expression of osteogenic TFs and genes. Moreover, we found that MACF1 regulated cytoplasmic-nuclear localization of itself, TCF12 and E2F6 in a concentration-dependent manner. MACF1 oppositely regulates the expression of TCF12 and transcription factor 7 (TCF7), two TFs that drive osteoblast differentiation to opposite directions. This study reveals that MACF1, a cytoskeletal protein, acts as a sponge for repressors of osteoblast differentiation to promote osteoblast differentiation and contributes to a novel mechanistic insight of osteoblast differentiation and transcription dynamics.

These authors contributed equally: Lifang Hu, Chong Yin, Dong Chen

Edited by E. Baehrecke

Supplementary information The online version contains supplementary material available at https://doi.org/10.1038/s41418-021-00744-9.

✉ Yi Zhang
yizhang@ablife.cc

✉ Airong Qian
qianair@nwpu.edu.cn

[1] Laboratory for Bone Metabolism, Key Laboratory for Space Biosciences and Biotechnology, School of Life Sciences, Northwestern Polytechnical University, Xi'an, Shaanxi, China

[2] Xi'an Key Laboratory of Special Medicine and Health Engineering, School of Life Sciences, Northwestern Polytechnical University, Xi'an, Shaanxi, China

[3] Research Center for Special Medicine and Health Systems Engineering, School of Life Sciences, Northwestern Polytechnical University, Xi'an, Shaanxi, China

[4] NPU-UAB Joint Laboratory for Bone Metabolism, School of Life Sciences, Northwestern Polytechnical University, Xi'an, Shaanxi, China

[5] ABLife BioBigData Institute, Wuhan, Hubei, China

[6] Center for Genome Analysis, ABLife Inc., Wuhan, Hubei, China

Introduction

Osteoblast differentiation leading to bone formation is a multistep process controlled by a well-defined spatio-temporal genetic program [1–5], which is regulated by numerous factors. Cytoskeleton, mainly the microtubule and actin filament (F-actin), has been demonstrated to be involved in osteoblast differentiation as participating in various signaling pathways, including Wnt, bone morphogenetic protein (BMP), Hedgehog, and mitogen-activated protein kinase (MAPK) [6–11], which are crucial for osteoblast differentiation and bone formation. Alteration of cytoskeleton causes changes in osteoblast differentiation. Inhibition of microtubule assembly enhances osteoblast differentiation and bone formation by increasing BMP-2 expression [12], while depolymerization of microtubules and disorganized microtubule network inhibits osteoblast differentiation [13, 14]. Moreover, stabilization of F-actin and inhibition of actin polymerization exert promotion effect on osteoblast differentiation and bone formation [15–17]. However, inhibiting actin reorganization suppresses osteoblast differentiation and bone formation [18]. These findings indicate that cytoskeleton is involved in osteoblast differentiation and

modulation of cytoskeleton dynamics results in changes in osteoblast differentiation.

Microtubule actin crosslinking factor 1 (MACF1) is a multidomain cytoskeletal protein that belongs to spectraplakin family [19–21]. As a scaffolding protein linking both microtubule and F-actin, MACF1 is crucial for cytoskeleton dynamics and widely involved in cell functions, including cell migration, proliferation, and differentiation [22–27]. We have found that MACF1 colocalizes with microtubule and F-actin in osteoblastic cells and regulates the distribution of microtubule and F-actin [24, 28]. Moreover, MACF1 promotes osteoblast differentiation and bone formation by altering osteogenic gene expression [29–31], however, a comprehensive understanding of the underlying mechanism remains unexplored.

In the current study, we report a comprehensive study of MACF1 regulating osteoblast differentiation. We found that MACF1 knockdown changed the normal transcriptional pattern of osteogenic genes and the down-regulated genes were mostly enriched in the osteoblast-differentiation-related functions and the regulation was dynamics. In addition, we identified two MACF1-interacted proteins (cyclin-dependent kinase 12 (CDK12), MYST/Esa1-associated factor 6 (MEAF6)) and two MACF1-interacted transcription factors (TFs) (transcription factor 12 (TCF12), E2F transcription factor 6 (E2F6)) as repressors of osteoblast differentiation. We further demonstrated that MACF1 regulated the cytoplasmic-nuclear localization of itself and TCF12 and E2F6 in a concentration-dependent manner, which contributes to the transcriptional dynamics. These findings indicate that MACF1 promotes osteoblast differentiation by sequestering the repressors in cytoplasm to facilitate the osteogenic genes expression.

Collectively, our findings extend our understanding of cytoskeletal protein and provide new knowledge about the regulation of osteoblast differentiation.

Materials and methods

Cell culture and transfection

The murine MC3T3-E1 osteoblastic cell line was a kind gift from Dr. Hong Zhou of the University of Sydney and grown in alpha-Minimum Essential Medium (α-MEM) (Life Technologies, Thermo Fisher Scientific, Carlsbad, CA) supplemented with 2.2 g/l sodium bicarbonate, 10% fetal bovine serum (FBS) (Biological Industries, Kibbutz Beit Haemek, Israel), 100 μg/ml streptomycin and 100 units/ml penicillin. The stable murine MACF1 knockdown (MACF1-KD) osteoblastic cell line and the corresponding Control cell line were generated by lentivirus-mediated short-hairpin RNA (shRNA) technology as reported previously [24] and cultured in α-MEM supplemented with 2.2 g/l sodium bicarbonate, 10% FBS, 100 μg/ml streptomycin and 100 units/ml penicillin. Human SaOS-2 osteoblast-like cell line was purchased from Procell Life Science & Technology Co., Ltd (Wuhan, China) and maintained in McCoy's 5 A medium (Procell Life Science & Technology Co., Ltd, Wuhan, China) supplemented with 15% FBS (Genetimes Excell Technology, Montevideo, Uruguay), 100 μg/ml streptomycin and 100 units/ml penicillin. All cells were cultured at humidified, 37 °C, 5% CO_2 incubator. For osteoblast differentiation, confluent cells were cultured with osteogenic medium which contained the culture medium supplemented with 50 μg/ml ascorbic acid (AA) (Sigma-Aldrich, St Louis, MO, USA) and 10 mM β–glycerophosphate (β-GP) (Sigma-Aldrich, St Louis, MO, USA) and the medium was changed every 2 days.

To knock down the expression of CDK12, MEAF6, TCF12, and E2F6 in cells, MC3T3-E1 cells were transfected with CDK12-siRNA, MEAF6-siRNA, TCF12-siRNA, E2F6-siRNA, and their corresponding control siRNAs (Ribobio, Guangzhou, China) respectively by using Lipofectamine 2000 Reagent (Life Technologies, Shanghai, China). To knock down the expression of MACF1 in SaOS-2 cells, SaOS-2 cells were transfected with MACF1-siRNA and its corresponding control siRNA (RQCON Biological Technology Co., Ltd, Xi'an, China) respectively by using Lipofectamine 2000 Reagent (Life Technologies, Shanghai, China).

Alkaline phosphatase staining

Alkaline phosphatase (ALP) of osteoblasts was stained by using BCIP (5-bromo-4-chloro-3-indolyl phosphate)/NBT (nitro blue tetrazolium) Alkaline Phosphatase Color Development Kit (Beyotime Biotechnology, Shanghai, China) according to the manufacturer's instruction. Briefly, cells were fixed in 10% buffered formaldehyde for 20 min, followed by washing with phosphate-buffered saline (PBS, pH7.4) for three times, 5 min/times, then were stained using BCIP/NBT solution. The staining reaction was stopped by washing with distilled water and the cell staining was imaged by a scanner (CanoScan 9000 F Mark II, Canon, Thailand).

Alizarin red s staining

Mineralized nodules were detected by alizarin red s (ARS, Sigma-Aldrich, St Louis, MO, USA) staining as previously described [29]. Briefly, cell cultures were fixed with 4% paraformaldehyde for 15 min, rinsed with PBS, and then stained with 0.5% ARS (pH4.2) for 15 min at room temperature. After washing with tap water for four times of 5 min each time, the mineralized nodules were imaged by a scanner (CanoScan 9000 F Mark II, Canon, Thailand).

Table 1 Primer sequences used for real-time PCR.

Gene name (species)	Primer sequences (5′- 3′)	Annealing temperature (°C)
ALP (mouse)	F: GTTGCCAAGCTGGGAAGAACAC R: CCCACCCCGCTATTCCAAAC	58
Runx2 (mouse)	F: TGCACCTACCAGCCTCACCATAC R: GACAGCGACTTCATTCGACTTCC	58
TCF7 (mouse)	F: CAGAATCCACAGATACAGCA R: CAGCCTTTGAAATCTTCATC	60
LEF1 (mouse)	F: GATCCCCTTCAAGGACGAAG R: GGCTTGTCTGACCACCTCAT	60
Col Iα1 (mouse)	F: GAAGGCAACAGTCGATTCACC R: GACTGTCTTGCCCCAAGTTCC	58
CDK12 (mouse)	F: CTGAATAACAGCGGGCAAAT R: AGCTCTGGAGGTCGATACCA	60
MEAF6 (mouse)	F: TGCCTCTTTGGCTTCTTGAT R: AGCTTCTTGTTCCTCCCACA	60
TCF12 (mouse)	F: TCAAAGCAACTGGTCAGCAC R: ATTGTGCAGAAGCGACACAC	60
E2F6 (mouse)	F: TGTGATTTGGTCCTGGTGAA R: GGGTACAATGCACAGGAGGT	60
GAPDH (mouse)	F: TGCACCACCAACTGCTTAG R: GGATGCAGGGATGATGTTC	60

Real-time PCR

Total RNA was extracted from cells using either TRIzol reagent (Invitrogen, Thermo Fisher Scientific, Carlsbad, CA) or Total RNA Kit I (Omega Bio-tek, Georgia, USA) according to the manufacturer's instruction. After extraction, 1 μg of total RNA sample was reverse transcribed into complementary DNA (cDNA) using PrimeScript™ RT reagent kit (Perfect Real Time) (TaKaRa, Dalian, China). The expression of genes was detected by real-time PCR carried out in C1000™ Thermal Cycler (Bio-Rad Labs, Hercules, CA) with specific primers (Tables 1 and S1) and SYBR Premix Ex Taq™ (TaKaRa). Samples were amplified using the following program: pre-denaturation at 95 °C for 30 s, followed by 45 cycles of 95 °C for 10 s, 58 °C or 60 °C for 30 s, and 72 °C for 5 s. Fluorescence detection was performed at the annealing phase at 80 °C to exclude the interference of primer dimer. The relative expression was calculated via $2^{-\Delta\Delta Ct}$ method [32] by using glyceraldehyde-3-phosphate dehydrogenase (*GAPDH*) for normalization of the threshold cycle (Ct) value.

Western blot

For western blot detection of protein levels, cellular total protein extracts were prepared on ice using Cell Lysis Buffer (Beyotime Biotechnology, Shanghai, China) supplemented with 1% Protease Inhibitor Cocktail Set III (Merck, Kenilworth, NJ). Nuclear and cytoplasmic protein extracts were prepared using a Nuclear and Cytoplasmic Extraction Kit (Pioneer Biotechnology, Xi'an, China). The protein concentration was determined by using BCA protein assay kit (Pioneer Biotechnology, Xi'an, China) and an equal amount of proteins for each sample was subjected to 6% (for MACF1) or 12.5% (for other proteins) SDS-PAGE and transblotted to nitrocellulose membrane (PALL Corporation, Port Washington, NY, USA). After incubation with the blocking buffer (5% nonfat milk), the membrane was incubated with appropriate primary antibodies against the following proteins in accordance with the manufacturer's instructions: runt related transcription factor 2 (Runx2) (8486, Cell Signaling Technology, Danvers, MA, USA), Osterix (AF7580, Affinity Biosciences, Jiangsu, China), transcription factor 7 (TCF7) (2203, Cell Signaling Technology, Danvers, MA, USA), lymphoid enhancer-binding factor 1 (LEF1) (14972-1-AP, Proteintech, Wuhan, China), CDK12 (ab37914, Abcam, Cambridge, MA, USA), MEAF6 (26465-1-AP, Proteintech, Wuhan, China), MACF1 (ab117418, Abcam, Cambridge, MA, USA, or Proteintech, Wuhan, China), TCF12 (ab201573, Abcam, Cambridge, MA, USA), E2F6 (ab53061, Abcam, Cambridge, MA, USA), Lamin B1 (12987-1-AP, Proteintech, Wuhan, China) and GAPDH (60004-1-Ig, Proteintech, Wuhan, China) at 4 °C overnight. The horseradish peroxidase (HRP) conjugated secondary antibody was further used (Pierce, Rockford, IL, USA). Protein bands were visualized by chemiluminescence using an ECL kit (Pioneer Biotechnology, Xi'an, China) and exposed to X-ray film. Protein band intensities were quantified using Image J software (National Institutes of Health, NIH). The GAPDH was used as the internal control for total protein and cytoplasmic protein, and Lamin B1 was used as the internal control for nuclear protein.

RNA-seq sample preparation and analysis

After extracting RNA from cells, total RNA was treated with RQ1 DNase (Promega, Fitchburg, WI) to remove DNA. The quality and quantity of the purified RNA were determined by measuring the absorbance at 260 nm/280 nm (A260/A280) using smartspec plus (Bio-Rad, CA, USA). RNA integrity was further verified by 1.5% agarose gel electrophoresis.

For each sample, 5 μg total RNA was used for RNA-seq library preparation (Gnomegen, California, USA). Polyadenylated RNAs were purified and concentrated with oligo (dT)-conjugated magnetic beads (Thermo Fisher Scientific, Waltham, MA, USA) prior to use for directional RNA-seq library preparation. Purified mRNAs were iron fragmented at 95 °C followed by end repair and 5′-adapter ligation. Next, reverse transcription was performed with RT primer

harboring a 3′-adapter sequence and randomized hexamer using RT Master mix (Gnomegen, California, USA), with the reaction conditions: 25 °C, 10 min, 42 °C, 40 min, 70 °C, 15 min, cool to 4 °C. The cDNAs were purified and amplified, and polymerase chain reaction (PCR) was performed using 2× HiFi PCR Master Mix (Gnomegen, California, USA) with the reaction conditions as below: 98 °C 45 s, 98 °C 15 s, 60 °C 30 s, 72 °C 30 s, 13 cycles. PCR products corresponding to 200–500 bps were collected by Size Selector (Gnomegen, California, USA), quantified, and stored at −80 °C until used for sequencing.

For high-throughput sequencing, the libraries were prepared following the manufacturer's instructions and applied to NextSeq 500 system for 151 nt pair-end sequencing (ABLife Inc., Wuhan, China).

After obtaining the raw sequenced reads, we firstly discarded raw reads containing unknown bases (N). Then sequencing adapters and the low-quality bases (quality score <20) were trimmed from raw sequencing reads using FASTX-Toolkit (Version 0.0.13). The short reads <16 nt were also dropped. Quality control for the filtered reads in fastq format was performed with FastQC (Version 0.9.5). Then filtered reads were aligned to the mouse GRCm38 genome (https://www.gencodegenes.org/mouse/) by TopHat2 [33] with four mismatches. Aligned reads with multiple genomic locations were removed, and only the reads with unique genomic location were kept for the following analysis. The RPKM (reads per kilobase and per million) value for each gene was calculated. Other statistical results, such as gene coverage and depth, reads distribution around transcription start sites (TSSs) and transcription terminal sites (TTSs), were also obtained. The maSigPro [34] package from Bioconductor was used to identify differentially expressed genes (DEGs) in measured time-courses with FDR ≤ 0.05 as threshold. The edgeR [35] package was also used to determine the DEGs for sample comparisons, based on the fold change (fold change ≥2 or ≤0.5) and false discovery rate (FDR ≤ 0.05) as thresholds.

Luciferase reporter assay

To analyze the activities of TFs TCF7 and TCF12, 8 repeats of each TF's motif sequence have been inserted to the promoter region of nanoluc luciferase gene sequence in PNL1.1 plasmid (N1351, Promega, Fitchburg, WI). MC3T3-E1 cells were seeded on a 12-well plate at 4×10^5 cells/well and cultured with α-MEM medium supplemented with 10% FBS overnight. Nanoluc luciferase reporter plasmid was transfected into MC3T3-E1 cells using Engreen Entranster™ H4000 Reagent (Engreen, 4000-6, Beijing, China), with blank nanoluc luciferase plasmid as normal control. Then the cells were transfected with siRNAs (CDK12-siRNA, MEAF6-siRNA, TCF12-siRNA, E2F6-siRNA) and negative control siRNA, respectively. A luciferase reporter assay was performed using the Nano-Glo® Luciferase Assay System (Promega, N1120, Fitchburg, WI) according to the manufacturer's instruction. Briefly, 100 µl cell culture medium was collected into a microplate, then 100 µl diluted Nano-Glo® Luciferase Assay Substrate was added. Nanoluc luciferase luminescent signals were quantified by a microplate reader (Synergy, USA) at 460 nm, and each value from the nanoluc luciferase constructs was normalized by a normal control.

Co-immunoprecipitation (Co-IP) and mass spectrometry (MS)

After verification of the specificity and IP ability of MACF1 antibody (ab117418, Abcam, Cambridge, MA, USA), the Control and MACF1-KD cells were adopted for Co-immunoprecipitation (Co-IP) and mass spectrometry (MS) assays. Cells were digested with 0.25% trypsin and collected after centrifugation with PBS washing. The cells were resuspended with NP-40 lysis buffer (50 mM Tris (pH7.4), 150 mM NaCl, 1% NP-40, 1 mM PMSF, 1 × protease inhibitor cocktail) and lysed on ice for 30 min. The cell lysate was mixed with MACF1 antibody and the antibody-lysate mix was incubated on a turning wheel overnight at 4 °C. Pierce™ Protein A/G Magnetic Beads (Thermo Fisher Scientific, Waltham, MA, USA) were washed with NP-40 lysis buffer for three times, and were added to the antibody-lysate complex and incubated on turning wheel for 2 h at 4 °C. After applying to magnet and removing the supernatants, the beads were washed with NP-40 lysis buffer for 4 times, 10 min/times, and the immunoprecipitates were eluted from the beads with elution buffer (50 nM Tris 8.0, 10 mM EDTA, and 1% SDS). After confirming the IP efficiency by Western blot, the eluted samples were detected by tandem mass spectrometer Q Exactive HF-X (Thermo Fisher Scientific, San Jose, CA, USA). Based on the UniProt mouse protein database, protein pilot software (SCIEX, Framingham, MA, USA) was used for protein matching analysis of MS results and the MACF1-interacted proteins were obtained.

Chromatin immunoprecipitation sequencing (ChIP-seq) and analysis

Samples were placed in tubes containing 1% paraformaldehyde (PFA) and fixed for 10 min. Glycine (1.25 M) was then added for 5 min to stop the reaction followed by centrifugation and wash with PBS to remove PFA. Samples were harvested with RIPA buffer (1% NP-40, 0.1% SDS, 0.5% sodium deoxycholate, 1 × PBS, 2% phenylmethylsulfonyl fluorid (PMSF) and 1 × protease inhibitor cocktail) followed by sonication on ice (15 min with

10 s pulse-on and 10 s pulse-off, 20% amplitude). DNA was sonicated to 200–500 bp. The lysate was then incubated with MACF1 antibody (ab117418, Abcam, Cambridge, MA, USA) at 4 °C overnight. The immunoprecipitates were further incubated with Pierce™ Protein A/G Magnetic Beads (Thermo Fisher Scientific, Waltham, MA, USA) for 2 h at 4 °C. After applying to magnet and removing the supernatants, we washed beads once with Low Salt Immune Complex wash buffer (0.1% SDS, 1% Triton X-100, 2 mM EDTA, 20 mM Tris-HCl, pH 8.1, 150 mM NaCl) and added 1 ml of buffer to each tube, rotated at 4 °C for 5 min. We then placed the tube on the magnet for 30 s, then discarded the supernatant. We repeated washing first with high salt immune complex wash buffer (0.1% SDS, 1% Triton X-100, 2 mM EDTA, 20 mM Tris-HCl, pH 8.1, 500 mM NaCl) and LiCl immune complex wash buffer (0.25 M LiCl, 1% IGEPAL-CA630, 1% deoxycholic acid (sodium salt), 1 mM EDTA, 10 mM Tris, pH 8.1) and second with TE Buffer (10 mM Tris-HCl, 1 mM EDTA, pH 8.0) for a total of five washes. The immunoprecipitates were eluted from the beads with elution buffer (50 nM Tris 8.0, 10 mM EDTA, and 1% SDS) and incubated at 65 °C overnight. After sequential RNase A and proteinase K treatment, DNA fragments were purified by phenol extraction and ethanol precipitation. Chromatin immunoprecipitation and sequencing (ChIP-seq) was performed by using ThruPLEX® DNA-seq kit (Rubicon Genomics, Michigan, USA) according to manufacturer's instructions. The PCR products corresponding to 300–500 bps were gel purified, quantified, and stored at −80 °C until used for sequencing. ChIP-seq sequencing was performed on NextSeq500 platform with 151 bp paired-end sequencing. The IP DNA and matched input DNA were prepared based on two independent experiments.

For ChIP-seq data analysis, the strategy of raw reads filtering is the same with RNA-seq data. The filtered clean reads were aligned to the mouse GRCm38 genome (https://www.gencodegenes.org/mouse/) by Bowtie2 software [36] with no >1 mismatch in seed region. Only the reads with unique genomic location were used for the following analysis. To assess the quality of ChIP-seq data, we used standard criteria of the ENCODE consortia [37]. The fraction of reads falling within peak regions was measured by FRiP (fraction of reads in peaks) method. The irreproducible discovery rate (IDR) analysis methodology [37] was used to assess the replicate agreement. The normalized ratio between the fragment-length cross-correlation peak and the background cross-correlation (normalized strand coefficient, NSC) and the ratio between the fragment-length peak and the read-length peak (relative strand correlation, RSC), were used to assess the signal-to-noise ratios in a ChIP-seq experiment [38]. To identify the binding sites of MACF1, we used Model-based Analysis for ChIP-seq (MACS version1.4) [39] to obtain the binding sites. The input samples without immunoprecipitation were treated as background. DeepTools [40] was used for the assignment of genomic features, such as relative location to TSS to the peaks and visualization of binding profiles. HOMER (Hypergeometric Optimization of Motif EnRichment) software [41] was used to search the enriched binding motifs in peaks.

Duolinker PLA staining

To analyze the binding effect of MACF1 and TCF12/E2F6 in osteoblastic cells, MACF1-KD cells and Control cells were seeded into 96-well plates with coverslips at a density of 4×10^3 cells/cm^2. After 3 days' osteogenic differentiation, the binding of MACF1 and TCF12, and MACF1 and E2F6 was determined by duolinker PLA staining with Duolink® In Situ Red Starter Kit Mouse/Rabbit (DUO92101, Sigma-Aldrich, St Louis, MO, USA) according to the manufacturer's instruction. Briefly, cells were washed by PBS (pH7.4) and then fixed in 10% buffered formaldehyde, followed by permeated with 0.5% Triton X-100 (TBS), then the cells were blocked with blocking solution for 30 min at room temperature. For the binding effects of MACF1/TCF12, and MACF1/E2F6, the cells were incubated with either rabbit MACF1 antibody (1:40, ab117418, Abcam, Cambridge, MA, USA), mouse TCF12 antibody (1:10, ab201573, Abcam, Cambridge, MA, USA), or mouse E2F6 antibody (1:30, MABE57, Sigma-Aldrich, St Louis, MO, USA) overnight at 4 °C. The cells were further incubated with mixed anti-mouse IgG PLA probe and anti-rabbit IgG PLA probe (1:5, respectively). PLA probes were combined by ligase (0.025U/ul) and amplificated with Amplification Polymerase (0.125U/μl). The cell nuclei were counterstained by 4′,6-diamidino-2-phenylindole (DAPI, 1 μg/ml, Roche Life Science, USA). Duolink® Mounting Media was used to mount the coverslips. The cells were observed by laser scanning confocal microscope (Leica TCS SP5, Wetzlar, Germany).

Immunofluorescence staining and laser scanning confocal microscopy

The Control and MACF1-KD osteoblastic cells were seeded on coverslips at a density of 2.5×10^4/cm^2, respectively. After growing confluence, the cells were cultured with osteogenic media for 3 days and the cellular distribution of MACF1, TCF12, E2F6, F-actin, and microtubules was detected by immunofluorescence staining. After wash with PBS, the cells were fixed with 4% paraformaldehyde for 15 min and permeated with 0.5% Triton X-100 (TBS) at room temperature. The cells were blocked with 2% bovine serum albumin (BSA) and 0.1% sodium azide in 0.1% Triton X-100 (TBS) for 10 min at room temperature. Then,

for detecting the distribution of MACF1, TCF12, and E2F6, the cells were incubated with either rabbit MACF1 antibody (1:40, ab117418, Abcam, Cambridge, MA, USA) and mouse TCF12 antibody (1:10, ab201573, Abcam, Cambridge, MA, USA), or rabbit MACF1 antibody and mouse E2F6 antibody (1:30, MABE57, Sigma-Aldrich, St Louis, MO, USA) overnight at 4 °C. For detecting the localization of MACF1, F-actin, and microtubules, the cells were incubated with either rabbit MACF1 antibody and cytopainter phalloidin-iFluor 488 reagent (1:1000, ab176753, Abcam, Cambridge, MA, USA), or rabbit MACF1 antibody and mouse α-tubulin antibody (1:80, 3873, Cell Signaling Technology, Danvers, MA, USA) overnight at 4 °C. After overnight incubation, the cells were further incubated with the corresponding secondary antibodies (goat anti-rabbit Cy3-IgG secondary antibody or goat anti-mouse FITC-IgG secondary antibody) for 1 h. DAPI Staining Solution (C1006, Beyotime Biotechnology, Shanghai, China) was used to counterstain cell nuclei for 10 min. Finally, the cells were enveloped with Fluoromount-G (Southern Biotech, USA). The stained cells were observed by laser scanning confocal microscope (Leica TCS SP5, Wetzlar, Germany). Cy3 (red fluorescence), FITC (green fluorescence), and DAPI (blue fluorescence) were excited at a wavelength of 543 nm, 488 nm, and 405 nm, respectively.

Statistical analysis

RNA-seq and ChIP-seq were independently performed for twice and other experiments were independently performed for three times. The statistical analysis of the data was performed with GraphPad Prism version 6.0 software (GraphPad Software Inc, La Jolla, CA). Significance of differences between two groups was evaluated with Student *t*-test. The data are presented as mean ± standard deviation (SD). Statistical significance was set at $p < 0.05$ ($^{*}p < 0.05$; $^{**}p < 0.01$; $^{***}p < 0.001$).

Results

MACF1 regulates the transcription dynamics of genes for osteoblast differentiation, bone mineralization and Wnt signaling

We previously found that MACF1 knockdown inhibited osteoblast differentiation from the beginning by altering the expression of *Runx2*, a key transcription factor for osteogenic differentiation [29]. Moreover, we found that MACF1 knockdown inhibited osteoblast differentiation in human osteoblast-like cells (SaOS-2 cell line), showing decreased ALP activity and mineralized nodules, and reduction of Runx2 and Osterix expression (Fig. S1). However, the comprehensive understanding of the underlying mechanism is still unclear. Here, we showed that MACF1 knockdown significantly decreased ALP activity (Fig. 1A) and mRNA level (Fig. 1B) after 0 day, 3 days, 5 days and 10 days osteoblast differentiation. The expressions of Runx2 and Osterix were also reduced in MACF1-KD cells during osteoblast differentiation (Fig. 1B, C).

To explore the potential mechanism of MACF1 inhibiting osteoblast differentiation, we performed whole-transcriptome analysis by high-throughput sequencing method (RNA-seq) for both Control and MACF1-KD cells, which were induced for osteoblast differentiation for 0 day, 3 days, 5 days, and 10 days, respectively (Fig. 1A). Sample correlation analysis revealed that except 10 days' samples, the global expression pattern between Control and MACF1-KD samples was distinctly separated (Fig. S2A). RNA-seq data showed that *Runx2* gene was suppressed in MACF1-KD cells at each time point compared to Control cells (Fig. S2B), suggesting the reliability of our data. We identified and clustered genes with dynamic expression patterns along the differentiation time points for Control cells and MACF1-KD cells by using updated maSigPro method [34]. Seven clusters for 7321 genes with dynamic expression patterns were revealed (Fig. 1D; Table S2, FDR (False Discovery Rate) ≤0.05). In the first cluster, genes showed increased level at 3 days and 5 days and decreased level at 10 days, and the varied pattern was more pronounced in Control group (Fig. 1D), which was coordinated with the *ALP* expression pattern in Fig. 1B. Moreover, genes in the seventh cluster showed consistently high levels in Control group compared with that in MACF1-KD group. Gene Ontology (GO) enrichment analysis revealed that these two clusters were enriched with DNA replication/cell cycle and translation biological processes, respectively, and both enriched with osteoblast differentiation term (Fig. 1D). For genes in cluster 2, 4, and 5, whose expression levels were higher in MACF1-KD group, were enriched with angiogenesis, barbed-end actin filament capping, and transcription related terms (Fig. 1D).

Further analysis of DEGs between MACF1-KD and Control cells showed that more up-regulated DEGs were induced by MACF1 knockdown at each detected time point of osteoblast differentiation (Fig. S2C). Gene ontology (GO) analysis of DEGs revealed that the most striking enrichment for osteoblast-differentiation-related categories such as osteoblast differentiation, ossification, and collagen fibril organization were associated with downregulated DEGs and the enrichments were decreased following differentiation process (Fig. 1E). Moreover, it was indicated that the alteration of expression patterns of osteoblast-differentiation-related genes occurred since 3 days' differentiation and was more significant on day 3 and day 5 time point (Fig. 1E). Besides, negative regulation of canonical

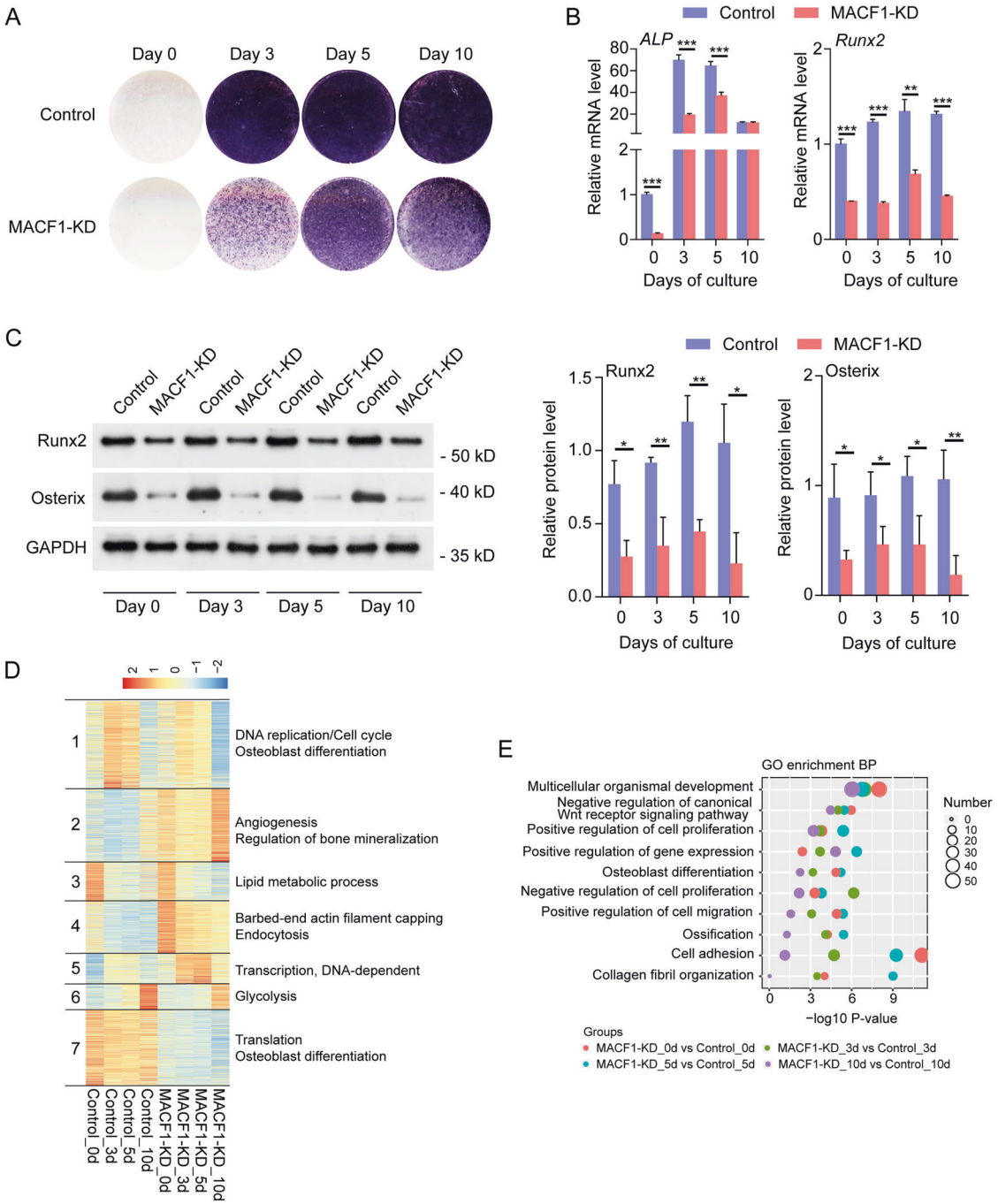

Fig. 1 MACF1 knockdown inhibits osteoblast differentiation and alters osteoblast differentiation transcriptome dynamics. A ALP activity of Control and MACF1-KD cells was detected by ALP staining. **B** The expression of *ALP* and *Runx2* examined by real-time PCR during osteoblastic differentiation in Control and MACF1-KD cells. Data represent mean value ± SD ($n = 3$). (**$P < 0.01$, ***$P < 0.001$). **C** The protein levels of Runx2 and Osterix determined by Western blot during osteoblastic differentiation in Control and MACF1-KD cells. Representative Western blots visualized by enhanced chemiluminescence method (left) and the quantification results with GAPDH as internal control (right) ($n = 3$). (*$P < 0.05$, **$P < 0.01$). **D** Heatmap showing the seven clusters of the differentially expressed genes (DEGs) identified by maSigPro program. The enriched GO biological process (BP) terms of each cluster were shown on the figure. **E** Bubble diagram showing the top 10 enriched GO BP terms for the downregulated genes during osteoblastic differentiation after MACF1 knockdown.

Wnt signaling pathway was significantly enriched in all four sample comparisons (Fig. 1E). These patterns of altered transcription were consistent with the striking difference in the phenotypic change after MACF1 knockdown. For the up-regulated genes in MACF1-KD cells, cell adhesion and angiogenesis-related terms were enriched (Fig. S2D).

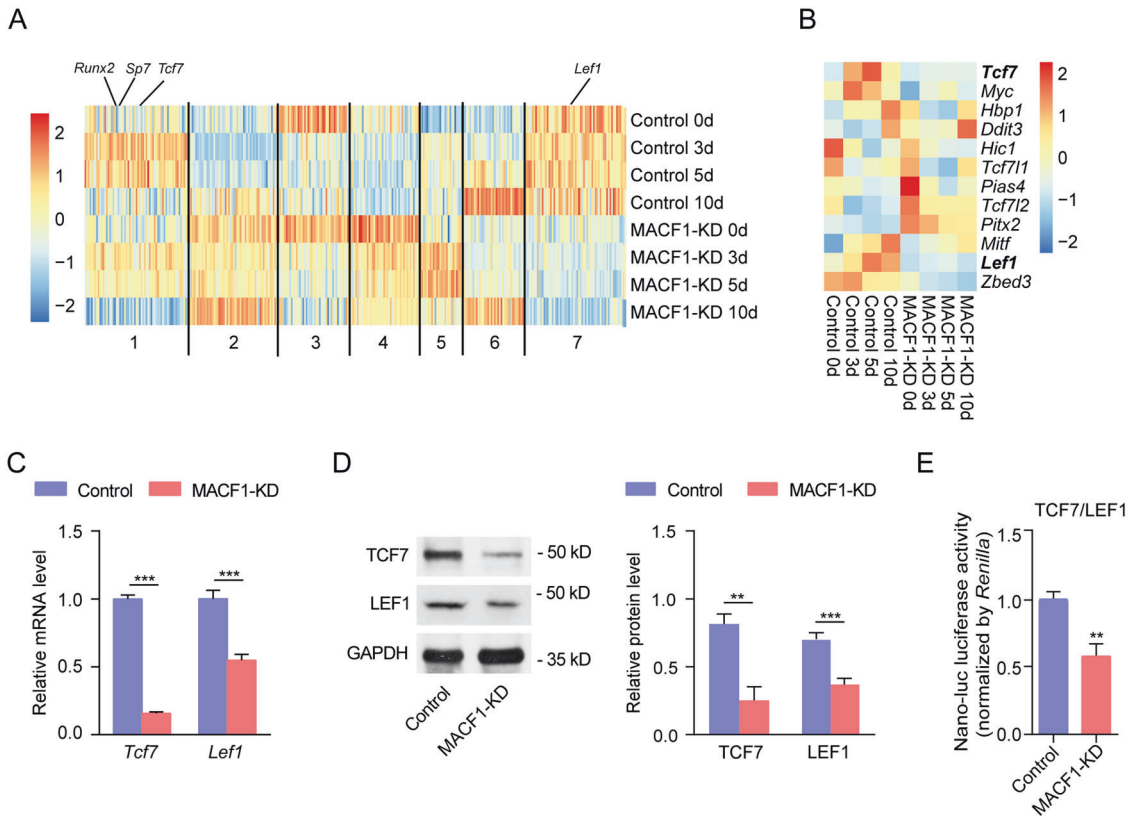

Fig. 2 MACF1 knockdown changes the expression profile of transcription factors during osteoblast differentiation. A Heatmap showing the differentially expressed transcription factors (TFs) between Control and MACF1-KD cells detected by maSigPro program. TFs were sorted by the rank of clusters. **B** Heatmap showing several key differentially expressed TFs in Wnt signaling pathway screened from (**A**). **C** Real-time PCR verification of the *Tcf7* and *Lef1* expression in Control and MACF1-KD cells. Data represent mean value ± SD ($n = 3$). (***$P < 0.001$) **D** Western blot verification of the TCF7 and LEF1 expression in Control and MACF1-KD cells. Representative Western blots visualized by enhanced chemiluminescence method (left) and the quantification results with GAPDH as internal control (right) ($n = 3$). (**$P < 0.01$, ***$P < 0.001$). **E** Luciferase reporter assay validation of the transcription activity of TCF7/LEF1 in Control and MACF1-KD cells. Data represent mean value ± SD ($n = 3$). (**$P < 0.01$).

These results together demonstrate that MACF1 deficiency alters the transcriptome dynamics of early-phase osteoblast differentiation.

Knockdown of MACF1 downregulates the expression of transcription factors (TFs) TCF7 and LEF1

TFs are critical for both osteoblast differentiation and its transcriptional program [42]. Thus, we analyzed the expression of TFs and obtained differentially expressed TFs (Fig. 2A; Table S3), among which Runx2 and Sp7 (Osterix) are two essential TFs known for osteoblast differentiation [42]. Their expression patterns belong to the cluster 1 (Fig. 2A). Figure 1E has indicated that MACF1-regulated genes were enriched in canonical Wnt signaling pathway. By screening the differentially expressed TFs that participate in the regulation of Wnt signaling pathway, we obtained several TFs (Fig. 2B). Among these differentially expressed TFs, TCF7 and LEF1 are two key mediators of Wnt signaling and play important role in regulating osteoblast differentiation [43], presenting low levels in MACF1-KD cells (Fig. 2B). Further experimental verification showed that MACF1 knockdown significantly downregulated the expression of TCF7 and LEF1 at both mRNA and protein level (Fig. 2C, D), and inhibited the transcription activity of TCF7/LEF1 (Fig. 2E). As TCF7 is critical for osteoblast differentiation by modulating the downstream osteogenic genes' expression, these results suggest that MACF1 may modulate the transcriptional program of osteoblast differentiation via TCF7 and LEF1.

Two MACF1-interacted proteins, CDK12 and MEAF6, are repressors of osteoblast differentiation and suppress expression of TCF7 and LEF1

The above results showed that the expression and transcription activity of TCF7 and LEF1 were regulated by MACF1.

To investigate how MACF1 affects TCF7 and LEF1, we performed co-immunoprecipitation (co-IP) for MACF1 and further detected the MACF1 physically interacted proteins using protein mass spectrometry assay. We identified 41 and 43 MACF1-interacted proteins in Control cells and MACF1-KD cells, respectively (Table S4). There were five proteins emerged in both Control cells and MACF1-KD cells (Fig. 3A), implying that the physically interacted proteins with MACF1 may be altered by MACF1 knockdown. By performing functional enrichment analysis of the MACF1-interacted proteins, we found that there were mainly intermediate filament and extracellular matrix (ECM) proteins who physically interact with MACF1 in Control cells (Fig. 3B), while nucleus was among the top enriched terms in MACF1-KD cells (Fig. 3B). Among the five proteins identified in both Control cells and MACF1-KD cells (Fig. 3A), actin (ACTB), vimentin (VIM), and histone H4 (HIST1H4A) all play roles in regulating osteoblast differentiation [15, 17, 44–46]. Different status of F-actin exerts either inhibitory or promotion effect on osteoblast differentiation [15–18], while vimentin inhibits osteoblast differentiation [44, 45]. Moreover, we also detected that MACF1 interacted with Dickkopf1 (DKK1) (Fig. 3A), which plays inhibitory effect on TCF7/LEF1 and osteoblast differentiation. Thus, we wondered if other MACF1-interacted protein functions in a similar way. To test this notion, we detected the function of CDK12 and MEAF6 in osteoblasts by knocking down them using small interfering RNA (siRNA) respectively (Fig. S3A–D). The results showed that knockdown of CDK12 significantly increased ALP activity and mineralized nodules (Fig. 3C), up-regulated the expression of osteogenic genes *Runx2* and type I collagen α1 (*Col Iα1*) (Fig. 3D), and the protein level of Runx2 and Osterix (Fig. 3E). In addition, knockdown of CDK12 significantly upregulated the expression of TCF7 and LEF1 at both mRNA level and protein level (Fig. 3F, G), and increased the TCF7/LEF1 transcription activity (Fig. 3H). Similar results were obtained for MEAF6. As shown in Fig. 3I, J, and K, knockdown of MEAF6 increased ALP activity, mineralized nodules, *Runx2* and *Col Iα1* gene expression, and Runx2 and Osterix protein levels. Moreover, knockdown of MEAF6 increased the expression of TCF7 and LEF1, and the TCF7/LEF1 transcription activity (Fig. 3L–N). These results indicate the inhibitory effect of CDK12 and MEAF6 on osteoblast differentiation and the expression of TCF7 and LEF1, suggesting that they are potential repressors of osteoblast differentiation.

Two MACF1-interacted TFs, TCF12 and E2F6, are repressors of osteoblast differentiation and suppress expression of TCF7 and LEF1

Co-IP together with protein mass spectrometry revealed that MACF1 could physically interacts with TFs (e.g., HES1, Table S4). Moreover, previous studies indicate the possibility of MACF1's localization in the nucleus [47]. These findings suggest that MACF1 might regulate gene transcription by directly interacting with osteoblast differentiation-related TFs. To test this hypothesis, we performed ChIP-seq for Control and MACF1-KD cells after 3 days' osteoblast differentiation, respectively. The binding profile around TSS region showed that in MACF1-KD cells, the MACF1 peaks were highly clustered near the TSS region (Fig. 4A), consistent with the hypothesis of the promoter binding via MACF1-TFs complex. However, in Control cells, no enriched MACF1 peaks around TSS region were evident (Fig. 4A). These data could be explained if the interaction between MACF1-TFs depends on the lower MACF1 expression level, which we will present below.

The MACF1-binding genes in MACF1-KD cells were further analyzed with KEGG pathway cluster analysis, and the results showed that Wnt signaling pathway was highly affected by MACF1 knockdown (Fig. 4B), which coincides with the RNA-seq results (Fig. 1E). The binding motifs of MACF1 complex were then searched by Homer software [41], which could find similar binding motifs of known TFs. Binding motifs of TCF12 were at the top of ranked motif by *P* value (Fig. 4C), and CA[GC]CT containing motifs were occupied the first top 8 motifs except the GC bias motif (Fig. S4). Besides, we also found the binding motif of E2F6, which was also presented with significant priority (Fig. 4C).

We then screened the potential binding targets of TCF12 and E2F6 by searching their binding motifs in the promoter region (see Methods for detailed information). By accumulating the binding density for the above-predicted targets of TCF12 and E2F6 in ChIP-seq data, we found that the binding densities of TCF12 and E2F6 within 10 kb of TSS were significantly enriched in MACF1-KD cells (Fig. 4D, E), further supporting that lower concentration of MACF1 is essential for the nuclear location of MACF1-TCF12 and MACF1-E2F6 and for their promoter binding activity.

To explore the function of TCF12 and E2F6 in osteoblast differentiation, we used siRNAs to knock down their expression, respectively (Fig. S5A–D). TCF12 or E2F6 knockdown significantly increased ALP activity, mineralized nodules, the mRNA level of *Runx2* and *Col Iα1*, and the protein level of Runx2 and Osterix (Fig. 4F–H, L–N). In addition, the expression of TCF7 and LEF1 (Fig. 4I, J, O, P) and the TCF7/LEF1 transcription activity (Fig. 4K, Q) were up-regulated upon TCF12 or E2F6 knockdown. These results reveal that TCF12 and E2F6 are repressors of osteoblast differentiation via repressing the expression of TCF7 and LEF1, which is similar to the repressor activities of CDK12 and MEAF6.

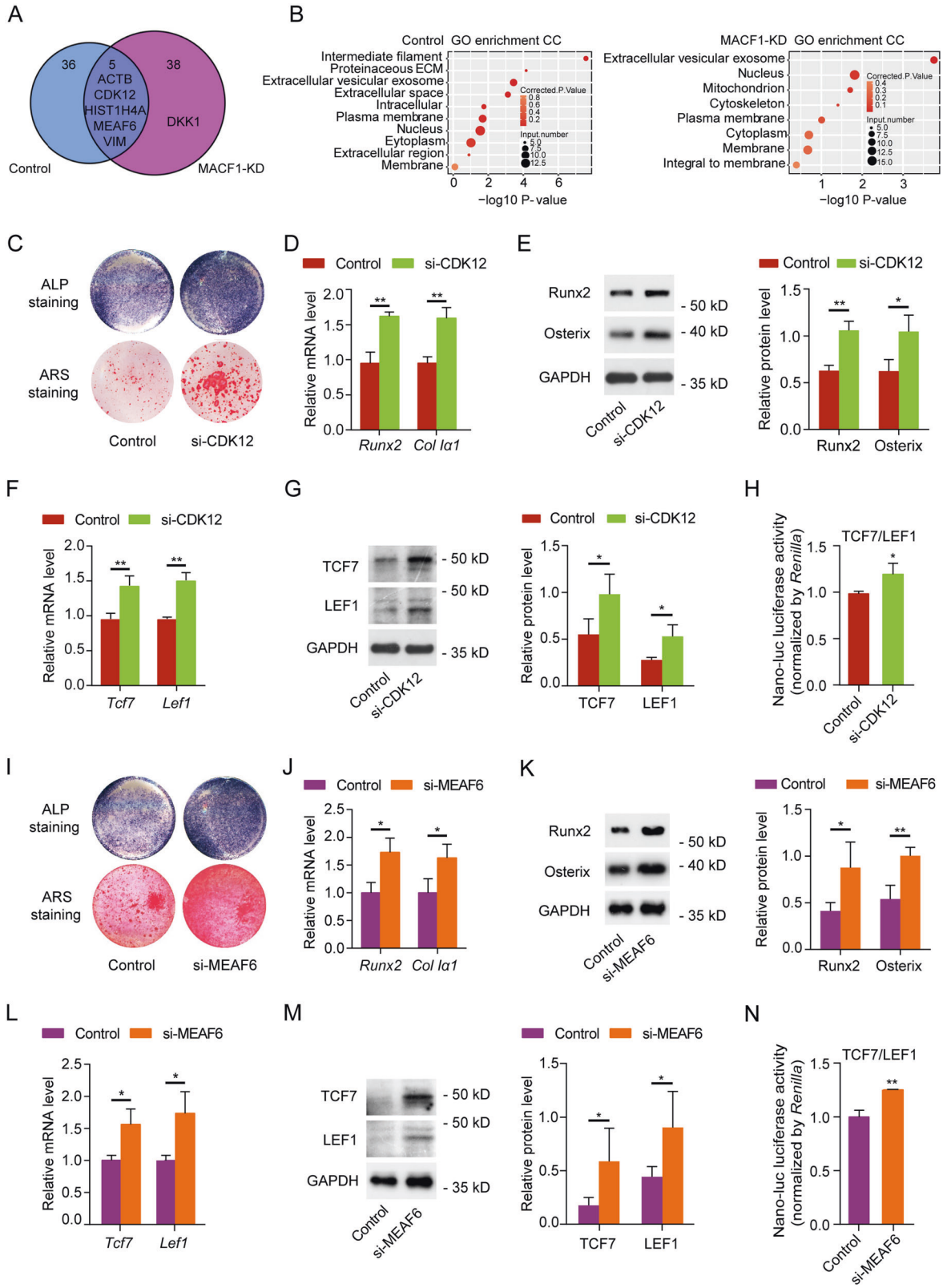
A
36
5
ACTB
CDK12
HIST1H4A
MEAF6
VIM
38
DKK1
Control
MACF1-KD
B
Control GO enrichment CC
Intermediate filament
Proteinaceous ECM
Extracellular vesicular exosome
Extracellular space
Intracellular
Plasma membrane
Nucleus
Cytoplasm
Extracellular region
Membrane
Corrected.P.Value
Input.number
−log10 P-value
MACF1-KD GO enrichment CC
Extracellular vesicular exosome
Nucleus
Mitochondrion
Cytoskeleton
Plasma membrane
Cytoplasm
Membrane
Integral to membrane
C
ALP staining
ARS staining
Control
si-CDK12
D
Control
si-CDK12
Relative mRNA level
Runx2
Col Iα1
E
Runx2
Osterix
GAPDH
- 50 kD
- 40 kD
- 35 kD
Relative protein level
F
Tcf7
Lef1
G
TCF7
LEF1
H
TCF7/LEF1
Nano-luc luciferase activity (normalized by Renilla)
I
si-MEAF6
J
K
L
M
N

◀ **Fig. 3 CDK12 and MEAF6 are identified as MACF1-interacted proteins, knockdown of which promotes osteoblast differentiation and upregulates the expression of TCF7 and LEF1. A** Venn diagram showing the overlapped MACF1-interacted proteins between Control and MACF1-KD cells detected by co-IP with protein mass spectrometry (MS). **B** Bubble diagram showing the top enriched GO cellular component (CC) terms for the detected proteins in Control (left panel) and MACF1-KD (right panel) cells, respectively. MC3T3-E1 osteoblasts were treated with or without CDK12 siRNA (si-CDK12) (**C**) or MEAF6 siRNA (si-MEAF6) (**I**) for ALP activity detection (ALP staining) and mineralized nodules formation determination (ARS staining) after 3 days' and around 19 days' osteoblast differentiation, respectively. The expression of osteogenic genes *Runx2* and *Col Iα1* examined by real-time PCR after si-CDK12 (**D**) or si-MEAF6 (**J**) treatment. Data represent mean value ± SD ($n = 3$). (*$P < 0.05$, **$P < 0.01$). The protein level of Runx2 and Osterix determined by Western blot after si-CDK12 (**E**) or si-MEAF6 treatment (**K**). Representative Western blots visualized by enhanced chemiluminescence method (left of **E**, **K**) and the quantification results with GAPDH as internal control (right of **E**, **K**) ($n = 3$). (*$P < 0.05$, **$P < 0.01$). The expression of *Tcf7* and *Lef1* examined by real time PCR after si-CDK12 (**F**) or si-MEAF6 (**L**) treatment. Data represent mean value ± SD ($n = 3$). (*$P < 0.05$, **$P < 0.01$). The protein level of TCF7 and LEF1 determined by Western blot after si-CDK12 (**G**) or si-MEAF6 (**M**) treatment. Representative Western blots visualized by enhanced chemiluminescence method (left of **G**, **M**) and the quantification results with GAPDH as internal control (right of **G**, **M**) ($n = 3$). (*$P < 0.05$). The transcription activity of TCF7/LEF1 was examined by luciferase reporter assay after si-CDK12 (**H**) or si-MEAF6 (**N**) treatment. Data represent mean value ± SD ($n = 3$). (*$P < 0.05$, **$P < 0.01$).

High level of MACF1 sequesters itself, TCF12 and E2F6 in cytoplasm

The above results demonstrate that TCF12 and E2F6 are MACF1-interacted TFs repressing osteoblast differentiation, and suggest that the nuclear interaction of MACF1 with TCF12 and E2F6 depends on a low MACF1 concentration. Duolinker PLA assay was performed to test this hypothesis, showing that MACF1 interacted with both TCF12 and E2F6 in cytoplasm under higher MACF1 expression level (Fig. 5A, B). In MACF1-KD cells, the cytoplasmic interaction was almost lost, while the nuclear interaction between MACF1 and TCF12 and E2F6 was evident, as reflected by the appearance of nuclear red spots (Fig. 5A, B).

Further immunofluorescence staining showed that in Control cells, MACF1 and E2F6 were mainly distributed in the cytoplasm, while TCF12 localized both in cytoplasm and in nucleus (Fig. 5C, D). In MACF1-KD cells, although total MACF1 amount was decreased, the nuclear amount of MACF1 increased, together with the increased amount of nuclear TCF12 and E2F6 (Fig. 5C, D).

In light of these findings, we speculated that high level of MACF1 might sequester TCF12 and E2F6, repressors of osteoblast differentiation, in cytoplasm and prevent them from translocating into nucleus. However, when MACF1 was reduced, TCF12 and E2F6 were translocated into the nucleus together with MACF1. To test this hypothesis, we detected the cellular localization of MACF1, TCF12, and E2F6 in Control and MACF1-KD cells by western blot. As shown in Fig. 5E, F, compared to Control group, there was significant increase of the nuclear fraction of MACF1, TCF12, and E2F6 in MACF1-KD cells. These results demonstrate that MACF1 regulates the cytoplasmic-nuclear localization of itself, TCF12 and E2F6, and support the hypothesis of the high concentration-dependent MACF1 sequestering mechanism.

Based on the above findings and the capacity of MACF1 in crosslinking microtubule and F-actin, we speculated that at high levels, MACF1 might bind to microtubule and F-actin cytoskeleton, which not only helps to maintain the normal distribution and organization of cytoskeleton but also sequesters MACF1 and its-interacted TFs in cytoplasm. However, at low levels, MACF1 interaction with microtubule and F-actin cytoskeleton is reduced, resulting in the altered cytoskeleton organization and an easy translocation into the nucleus together with its-interacted TFs. To verify this hypothesis, we detected the cellular localization of MACF1, F-actin and microtubules in Control and MACF1-KD cells by immunofluorescence staining. As shown in Fig. S6, in Control cells, MACF1 was mainly distributed in the cytoplasm and colocalized with F-actin filaments (Fig. S6A) and microtubules (Fig. S6B). The F-actin filaments were abundant and distributed at cell periphery or passed through the cytoplasm as rope-like structure (Fig. S6A) and microtubules bundles projected radially toward the cell periphery (Fig. S6B). However, in MACF1-KD cells, F-actin became less and were mainly localized at cell periphery (Fig. S6A) and microtubules became noncontinuous, curled, and bent (Fig. S6B). Meanwhile, the cytoplasmic distribution of MACF1 was largely reduced, no longer colocalizing with F-actin and microtubules, and the increase in the nuclear MACF1 was profound (Fig. S6A, B). These results reveal that MACF1 stably associates with cytoskeleton and supports the cytoskeleton structure in a concentration-dependent manner, which in turn retains MACF1 and MACF1-interacted proteins in cytoplasm.

MACF1 promotes TCF7 transcription by repressing TCF12 function

MACF1 promoted the transcription activity of TCF7/LEF1 (Fig. 2), while MACF1-interacted TCF12 inhibited the transcription activity of TCF7/LEF1 (Fig. 4), suggesting a relationship between these two events. By constructing the TCF7 and TCF12 nano-luc luciferase reporter plasmids (Fig. 6A), we detected the effects of MACF1 on the transcription activity of TCF12 and TCF7 in osteoblast differentiation. The results showed that in Control cells, upon osteoblast

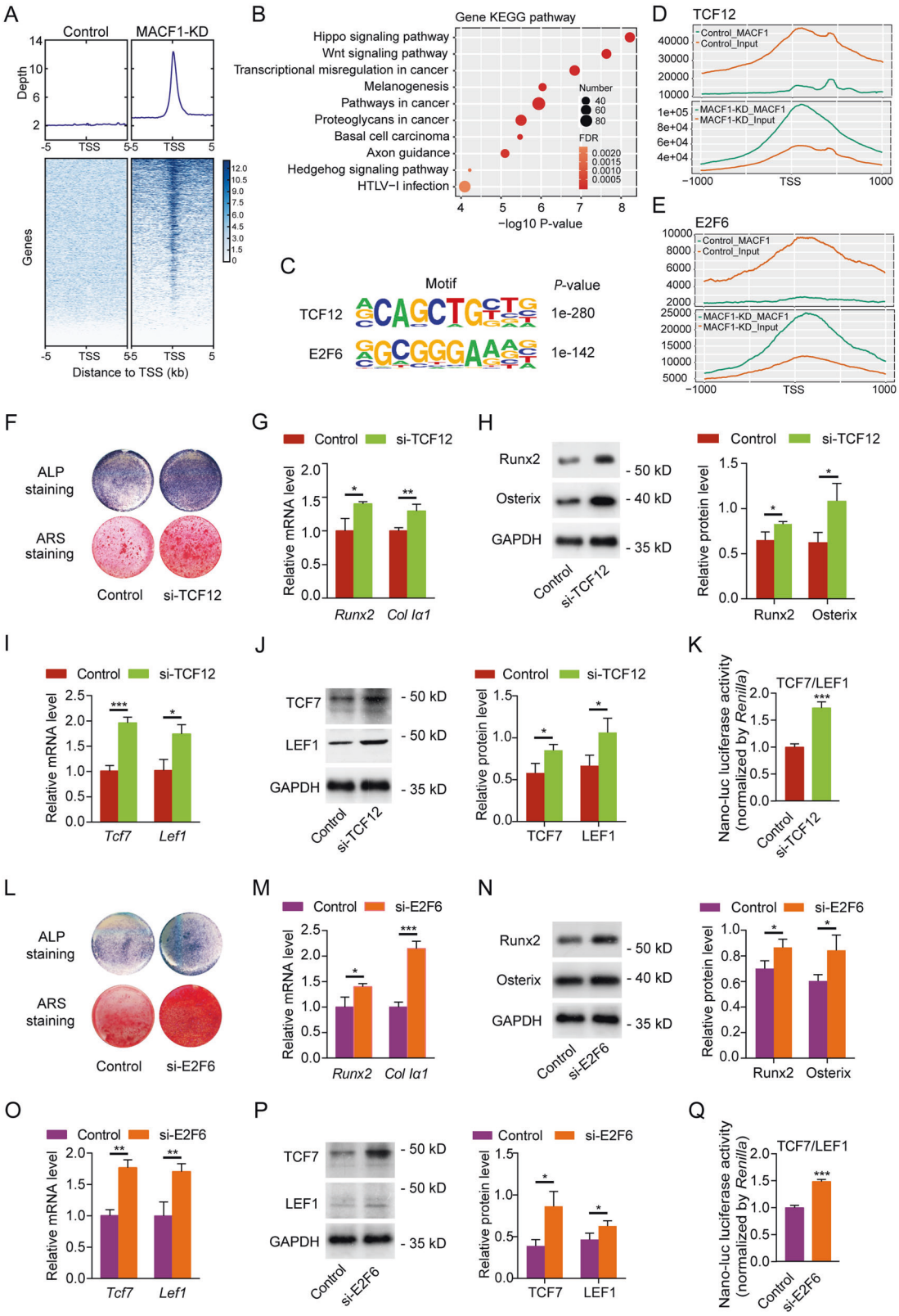

differentiation, TCF12's transcription activity decreased while TCF7's transcription activity increased (Fig. 6B, C). In contrast, in MACF1-KD cells, TCF12's transcription activity increased, while TCF7's transcription activity decreased (Fig. 6B, C). This finding suggests the opposite regulatory roles of MACF1 on the TCF12 and TCF7.

◀ **Fig. 4 Transcription factors (TFs) TCF12 and E2F6 are determined as MACF1-interacted TFs, knockdown of which promotes osteoblast differentiation and upregulates the expression of TCF7 and LEF1. A** Density and heatmap plot showing the binding profiles around TSS region for all genes in Control and MACF1-KD cells, respectively. **B** Bubble diagram showing the top KEGG pathways for the genes bound by MACF1 in MACF1-KD cells. **C** The binding motifs of two known TFs and their significant *p* values. The motifs were extracted from the binding peaks of MACF1 by Homer software in MACF1-KD cells. Line plot showing the enriched density for genes with binding motifs of TCF12 (**D**) or E2F6 (**E**) in MACF1-KD cells compared with Control cells detected by ChIP-seq. The input sample represented genomic DNA density without immunoprecipitation. MC3T3-E1 osteoblasts were treated with or without TCF12 siRNA (si-TCF12) (**F**) or E2F6 siRNA (si-E2F6) (**L**) for ALP activity (ALP staining) and mineralized nodules formation detection (ARS staining) after 3 days' and around 19 days' osteoblast differentiation, respectively. The expression of osteogenic genes *Runx2* and *Col Iα1* examined by real-time PCR after si-TCF12 (**G**) or si-E2F6 (**M**) treatment. Data represent mean value ± SD ($n = 3$). (*$P < 0.05$, **$P < 0.01$, ***$P < 0.001$). The protein level of Runx2 and Osterix determined by Western blot after si-TCF12 (**H**) or si-E2F6 treatment (**N**). Representative Western blots visualized by enhanced chemiluminescence method (left of **H**, **N**) and the quantification results with GAPDH as internal control (right of **H**, **N**) ($n = 3$). (*$P < 0.05$). The expression of *Tcf7* and *Lef1* examined by real-time PCR after si-TCF12 (**I**) or si-E2F6 (**O**) treatment. Data represent mean value ± SD ($n = 3$). (*$P < 0.05$, **$P < 0.01$, ***$P < 0.001$). The protein level of TCF7 and LEF1 determined by Western blot after si-TCF12 (**J**) or si-E2F6 treatment (**P**). Representative Western blots visualized by enhanced chemiluminescence method (left of **J**, **P**) and the quantification results with GAPDH as internal control (right of **J**, **P**) ($n = 3$). (*$P < 0.05$). The transcription activity of TCF7/LEF1 was examined by luciferase reporter assay after si-TCF12 (**K**) or si-E2F6 (**Q**) treatment. Data represent mean value ± SD ($n = 3$). (***$P < 0.001$).

Because MACF1 binds to TCF12, we further determined whether TCF12 was involved in MACF1-promoted TCF7's transcription activity. The results showed that the regulatory effect of MACF1 on TCF7's transcription activity disappeared when TCF12 was knocked down (Fig. 6D).

We then analyzed the enriched functional GO terms for the predicted bound genes of TCF12 and TCF7, and found they were both enriched in multicellular organismal development and bone mineralization terms for TCF12 and TCF7, respectively (Fig. 6E, F). These data together demonstrate that, although functionally opposite, both TCF12 and TCF7 are transcription factors targeting osteoblast differentiation, and TCF12 negative regulation of TCF7 expression is dampened by high level of MACF1.

Discussion

This study has identified two MACF1-interacted proteins (CDK12 and MEAF6) and two MACF1-interacted TFs (TCF12 and E2F6) as repressors of osteoblast differentiation. Our results demonstrate that MACF1 functions as a positive regulator of osteoblast differentiation by sequestering the repressors. Moreover, MACF1 regulates cytoplasmic-nuclear localization of itself and the suppressors TCF12 and E2F6 in a concentration-dependent manner, which may be related to the F-actin and microtubule cytoskeleton distribution and organization regulated by MACF1 level. This study contributes to a novel mechanistic insight of osteoblast differentiation and transcription dynamics.

MACF1, a broadly expressed scaffolding protein by linking both microtubules and actin, has been shown to be important for numerous cell functions, such as cell migration, proliferation, and differentiation [22–25]. We have previously revealed that MACF1 promotes osteoblast differentiation and bone formation [29, 30]. In this study, RNA-seq analysis of the Control and MACF1-KD cells under osteoblast differentiation revealed that MACF1-downregulated genes were mostly enriched in the osteoblast-differentiation-related functions and the regulation was dynamics, consistent with the current model that osteoblast differentiation is driven by unique spatial and temporal expression of functionally related genes [1, 2, 4, 5].

The RNA-seq results also confirmed our previous finding of MACF1 promoting the expression of *TCF7*, *LEF1,* and *Runx2* [29], indicating that MACF1 participates in the regulation of gene expression. Runx2 is the master regulator of osteoblastogenesis [5, 48]. Sp7/Osterix functions downstream of Runx2 and also regulates Runx2 expression [49–51]. TCF7 and LEF1 are best known as nuclear effectors of Wnt/β-catenin signaling, which is a key pathway promoting osteoblast differentiation. Runx2 directly regulates the expression of *TCF7* and TCF7 and β-catenin activate the P1 promoter and osteoblast-specific enhancer of *Runx2* [51–53]. MACF1 positive regulation of the expression of Runx2, Sp7/Osterix, TCF7, and LEF1 suggests that MACF1 is a master regulator of controlling the transcriptional dynamics of osteoblast differentiation, and also indicates the presence of a mechanism for MACF1 in supporting the expression of these key transcription factors.

To elucidate the mechanism of the mast role of MACF1 in controlling the osteoblast differentiation programs, we firstly applied proteomic approach which has identified five MACF1-interacted proteins (ACTB, CDK12, HIST1H4A, MEAF6, and VIM) emerged in both Control cells and MACF1-KD cells. As ACTB, VIM and HIST1H4A have been demonstrated roles in regulating osteoblast differentiation [15–18, 44–46], we detected the roles of CDK12 and MEAF6, two key regulators of cellular functions [54–57], in osteoblast differentiation. Further functional analysis revealed that both CDK12 and MEAF6 were repressors of osteoblast differentiation. It has reported that Runx2 harbors a conservative binding site for CDK family members [58, 59], and cyclin D1-CDK4 binds to Runx2 to induce it degradation, which inhibits osteoblast differentiation [59]. Our finding suggests that CDK12, a

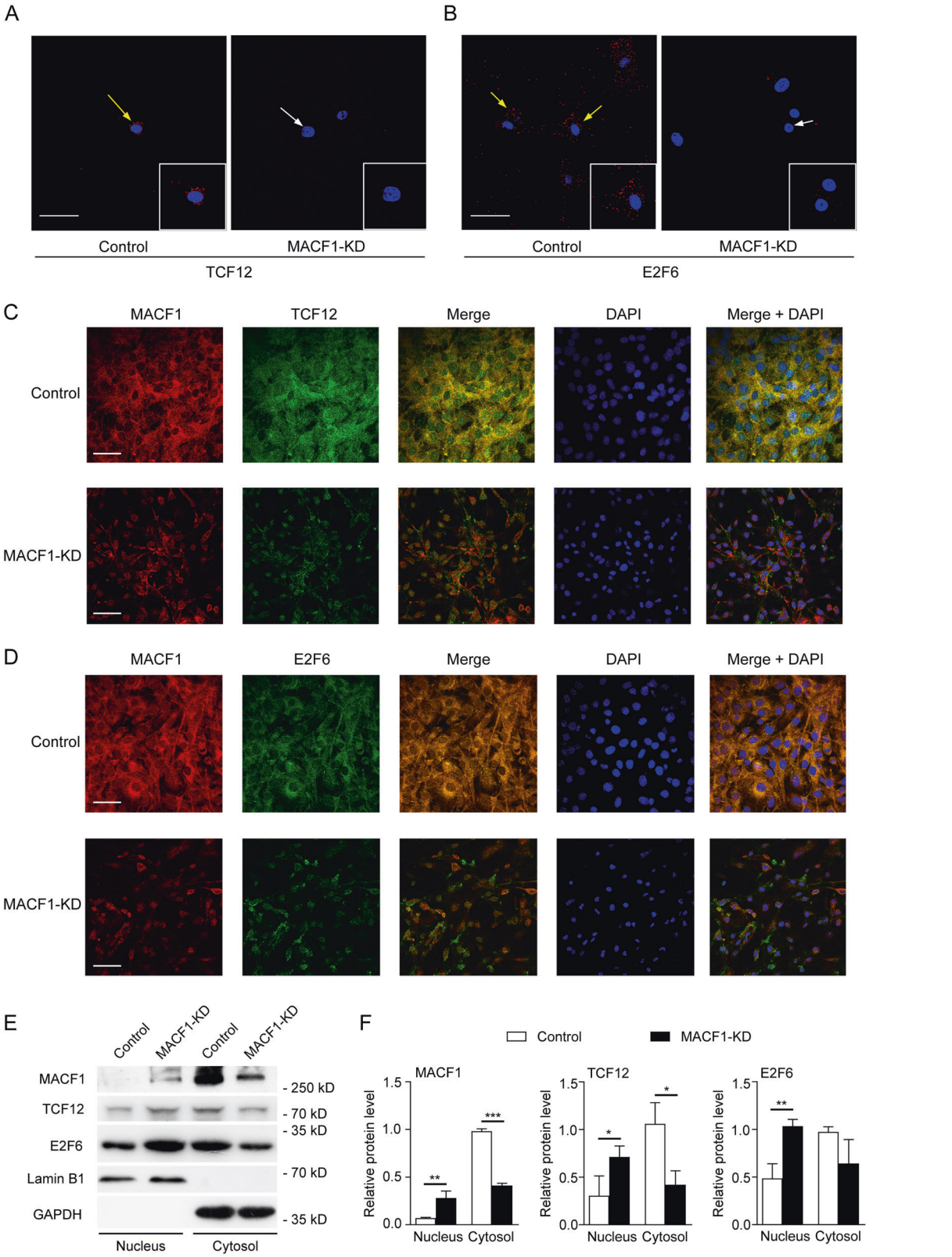

member of CDK family, may function similarly as does CDK4. MEAF6 is a molecular involved in cancer development [60, 61], while its function in regulating osteoblast differentiation has never been reported. Our findings firstly identified CDK12 and MEAF6 as repressors of osteoblast differentiation.

◀ **Fig. 5 MACF1 knockdown promotes the nuclear translocation of MACF1, TCF12, and E2F6. A**, **B** The interactions between MACF1 and TCF12, MACF1, and E2F6, were determined by duolinker PLA assay. Red staining (arrow) shows the interactions. Bar: 50 μm. **C**, **D** The cellular distribution of MACF1, TCF12, and E2F6, and the colocalization between MACF1 and TCF12, MACF1 and E2F6 detected by immunofluorescence staining. Bar: 50 μm. **E** Representative Western blots of the nuclear (nucleus) and cytosolic (cytosol) fractions of MACF1, TCF12, and E2F6. Lamin B1 and GAPDH were used as internal controls for nuclear and cytosolic fractions, respectively. **F** Quantification of nuclear and cytosol levels of MACF1, TCF12, and E2F6 with Lamin B1 and GAPDH as internal control, respectively. Data represent mean value ± SD ($n = 3$). (*$P < 0.05$, **$P < 0.01$, ***$P < 0.001$).

We further applied MACF1 ChIP-seq experiments to identify TFs that may cooperate with MACF1 to regulate gene expression, via analysis of their DNA binding sites. Two such TFs TCF12 [62] and E2F6 [63, 64] have been identified. Yi et al. have reported lately that knockdown of TCF12 promoted osteoblastic differentiation of mesenchymal stem cells (MSCs) while overexpression of TCF12 suppressed it [65]. Our functional analysis revealed both TCF12 and E2F6 as negative regulators of osteoblast differentiation. For the first time to our knowledge, the suppressor function of CDK12, MEAF6, and E2F6 in regulating osteoblast differentiation has been discovered. In light of these findings, we propose a model in which MACF1 promotes osteoblast differentiation by sequestering the repressors of this process (Fig. 7).

Although MACF1 is a cytoskeletal protein, Aguirre et al. have recently reported the nuclear localization of MACF1a in the oocyte of zebrafish [47], indicating the possibility of MACF1 translocating into the nucleus. In this study, we reveal that knockdown of MACF1 promotes the nuclear localization of both TCF12 and E2F6, as well as itself, suggesting that high-level MACF1 sequesters repressor TFs in cytoplasm to secure osteoblast differentiation. Consistent with this model, we showed that MACF1 oppositely regulates the expression of TCF12 and TCF7, two TFs that drive osteoblast differentiation to opposite directions. These findings extend our knowledge capacity that a cytoskeletal protein can act as a master transcriptional regulator by the concentration-dependent regulation of the nuclear translocation of its associated TFs and other regulatory proteins.

Interestingly, a number of proteins involved in regulating cytoskeleton structure have been demonstrated to play roles in regulating osteoblast differentiation. Microtubule-associated protein DCAMKL1 (Doublecortin-like and CAM kinase-like 1) suppresses osteoblast differentiation by promoting microtubule polymerization, which antagonizing Runx2 [66]. However, stathmin, a microtubule accessory protein that inhibits microtubule assembly, enhances osteoblast differentiation [67]. As DCAMKL1 is a different kind microtubule-associated protein compared with stathmin, these findings suggest a precise regulation of multiple proteins that control microtubule dynamics on osteoblast differentiation. Moreover, inhibition of cofilin 1 and destrin, two main actin-depolymerizing factors, results in stabilized F-actin and enhanced osteoblastic differentiation of human MSCs [15]. Our findings of the involvement of MACF1 in maintaining F-actin and microtubules' distribution and organization, and also supporting osteoblast differentiation, are in line with this scenario. In addition, Wang et al. have demonstrated that Kank, a protein regulating actin dynamics, is a nucleo-cytoplasmic shuttling protein that binds to β-catenin to enter into the nucleus together [68]. In this context, our findings of the concentration-dependent dynamics of the MACF1 cytoplasmic-nuclear localization and the similar dynamics of its associated TCF12 and E2F6, suggest a concentration-dependent nuclear shuttling mechanism of MACF1 and its associated regulatory proteins.

MACF1 has been demonstrated to interact with nesprin-3α (nuclear envelope spectrin repeat 3α) via its actin-binding domain (ABD) [69]. Nesprin-3α is a member of nesprin family that is component of LINC (linker of nucleoskeleton and cytoskeleton) complexes connecting cytoskeleton to the nuclear interior [70]. By interacting with nesprin-3α that is located at the nuclear envelope, MACF1 connects microtubules to the nucleus. According to our previous findings [24] and results from this study, MACF1 stably associates with cytoskeleton at high levels and the low level of MACF1 causes disorganization of F-actin and microtubule cytoskeleton, we thusly propose that MACF1 may stably associate with cytoskeleton and support the cytoskeleton structure in a concentration-dependent manner. This strong association retains other MACF1-interacting proteins including the differentiation suppressors TCF12, E2F6, MEAF6, and CDK12 in cytoplasm, when MACF1 concentration is high during differentiation. On the contrary, when MACF1 concentration is low during the undifferentiation state, MACF1 does not associate with cytoskeleton well. Consequently, MACF1 interaction with nesprin-3α, TCF12, and MEAF6 may allow an efficient translocation of MACF1 into nucleus.

In summary, MACF1, a cytoskeletal protein, effectively sequesters suppressive transcription regulators of osteogenic genes in cytoplasm to ensure successful osteoblast differentiation, while its down-regulation results in the nuclear translocation of repressors and shuts off the transcriptional program for osteoblast differentiation (Fig. 7). This provides a novel mechanism for effective switching on and off the transcription programs for differentiation of osteoblast and possibly of other cells. We propose that regulation of the nuclear shuttling of regulatory proteins by association with cytoskeleton and/or cytoskeleton-associated proteins

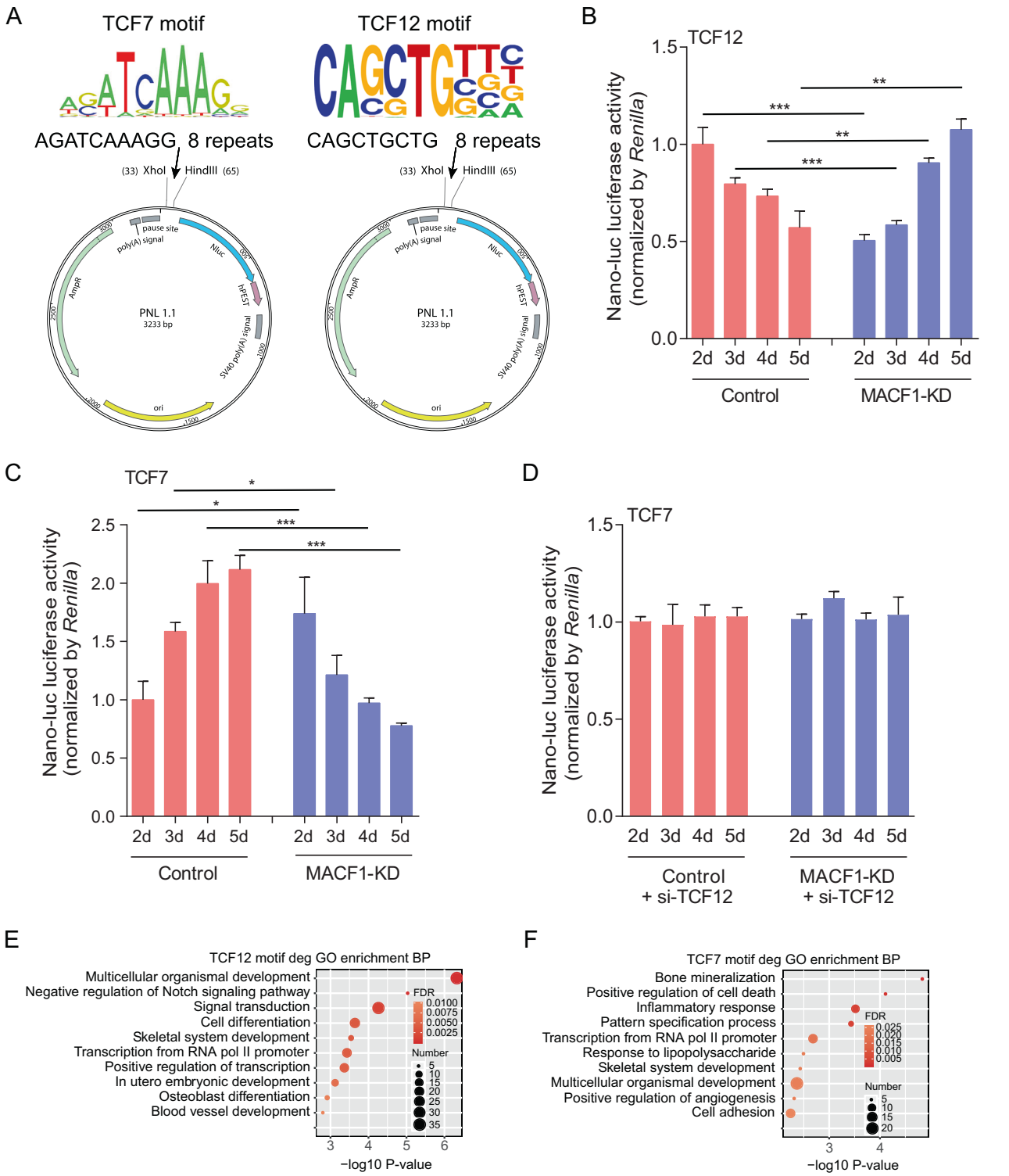

Fig. 6 MACF1 oppositely regulates the transcription activity of TCF12 and TCF7 to regulate their downstream genes expression. **A** Schematic illustration of the design of the TCF7 and TCF12 nano-luc luciferase reporter plasmids. **B** Transcription activity of TCF12 in Control or MACF1-KD cells detected by luciferase reporter assay. Data represent mean value ± SD ($n = 3$). Statistical analysis was performed using Student *t*-test compared to the corresponding control group (**$P < 0.01$, ***$P < 0.001$). **C** Transcription activity of TCF7 in Control or MACF1-KD cells detected by luciferase reporter assay. Data represent mean value ± SD ($n = 3$). Statistical analysis was performed using Student *t*-test compared to the corresponding control group (*$P < 0.05$, ***$P < 0.001$). **D** Transcription activity of TCF7 after TCF12 siRNA (si-TCF12) treatment in Control or MACF1-KD cells detected by luciferase reporter assay. Data represent mean value ± SD ($n = 3$). Bubble diagram showing the enriched GO BP terms for the DEGs downstream of TCF12 (**E**) and TCF7 (**F**).

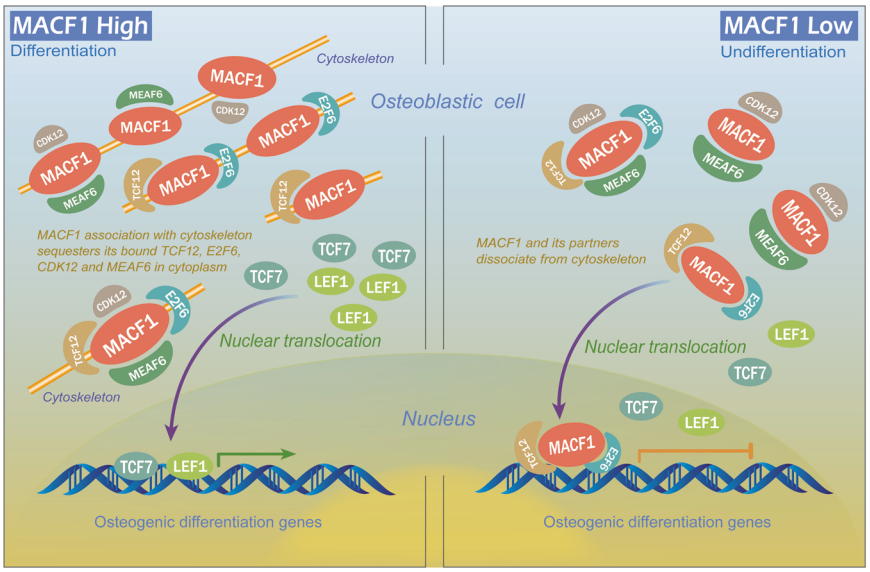

Fig. 7 Proposed model of MACF1 regulating osteoblast differentiation by sequestering the repressors in cytoplasm. MACF1 stably associates with cytoskeleton at high level and effectively sequesters suppressive transcription regulators of osteogenic genes in cytoplasm to ensure successful osteoblast differentiation, while low level of MACF1 results in the nuclear translocation of repressors and shuts off the transcriptional program for osteoblast differentiation.

may represent a general mechanism for switching on and off transcriptional programs in various biological processes. The novel mechanism of MACF1 in regulating osteoblast differentiation in mouse cells may be extended to human cells, as we have demonstrated the similar function of MACF1 in regulating human osteoblast differentiation in SaOS-2 cell line. If this is true, the present findings may shed light on developing new therapeutic applications in curing bone diseases.

Data availability

The sequenced RNA-seq and ChIP-seq data in this study have been deposited on NCBI Gene Expression Omnibus (GEO) database with an access number GSE120252. The data which support the findings of this study are available from the corresponding author on reasonable request.

Acknowledgements We thank Dr. Hong Zhou (The University of Sydney, Australia) for providing MC3T3-E1 cell line.

Funding This work was supported by the National Natural Science Foundation of China (81772017, 31570940, 82072106), the China Postdoctoral Science Foundation (2018T111099, 2017M610653), Young Talent Fund of University Association for Science and Technology in Shaanxi, China (20170401), The Project Supported by Natural Science Basic Research Plan in Shaanxi Province of China (2018JM3040), and the grant (BKJ17J004). This work was also supported by ABLife, Inc., Wuhan (201508001).

Author contributions LFH, CY, DC, YZ (Yi Zhang), and ARQ conceived and designed the study. LFH, CY, DC, ZXW, SJL, YZ (Yu Zhang), ZZH, SYL, XX, and ZHC performed experiments, analyzed data, and generated figures. All authors contributed to experimental design and manuscript writing. LFH, CY, DC, YZ (Yi Zhang), and ARQ revised manuscript. All authors have approved the final version to be published.

Compliance with ethical standards

Conflict of interest The authors declare no competing interests.

Ethics This study did not require ethical approval.

Publisher's note Springer Nature remains neutral with regard to jurisdictional claims in published maps and institutional affiliations.

References

1. Ducy P, Schinke T, Karsenty G. The osteoblast: a sophisticated fibroblast under central surveillance. Science. 2000;289:1501–1504.
2. Harada S, Rodan GA. Control of osteoblast function and regulation of bone mass. Nature. 2003;423:349–355.
3. Huang W, Yang S, Shao J, Li YP. Signaling and transcriptional regulation in osteoblast commitment and differentiation. Front Biosci. 2007;12:3068–3092.
4. Karsenty G, Kronenberg HM, Settembre C. Genetic control of bone formation. Annu Rev Cell Dev Biol. 2009;25:629–648.
5. Long F. Building strong bones: molecular regulation of the osteoblast lineage. Nat Rev Mol Cell Biol. 2011;13:27–38.
6. Salinas PC. Modulation of the microtubule cytoskeleton: a role for a divergent canonical Wnt pathway. Trends Cell Biol. 2007;17:333–342.
7. Xu H, Wu F, Zhang H, Yang C, Li K, Wang H, et al. Actin cytoskeleton mediates BMP2-Smad signaling via calponin 1 in preosteoblast under simulated microgravity. Biochimie. 2017;138:184–193.
8. Stegman MA, Vallance JE, Elangovan G, Sosinski J, Cheng Y, Robbins DJ. Identification of a tetrameric hedgehog signaling complex. J Biol Chem. 2000;275:21809–21812.
9. Galli C, Piemontese M, Lumetti S, Ravanetti F, Macaluso GM, Passeri G. Actin cytoskeleton controls activation of Wnt/beta-catenin signaling in mesenchymal cells on implant surfaces with different topographies. Acta Biomater. 2012;8:2963–2968.
10. Sonowal H, Kumar A, Bhattacharyya J, Gogoi PK, Jaganathan BG. Inhibition of actin polymerization decreases osteogeneic

differentiation of mesenchymal stem cells through p38 MAPK pathway. J Biomed Sci. 2013;20:71.
11. Hirata H, Gupta M, Vedula SR, Lim CT, Ladoux B, Sokabe M. Quantifying tensile force and ERK phosphorylation on actin stress fibers. Methods Mol Biol. 2017;1487:223–234.
12. Zhao M, Ko SY, Liu JH, Chen D, Zhang J, Wang B, et al. Inhibition of microtubule assembly in osteoblasts stimulates bone morphogenetic protein 2 expression and bone formation through transcription factor Gli2. Mol Cell Biol. 2009;29:1291–1305.
13. Shi W, Zhang Y, Chen K, He J, Feng X, Wei W, et al. Primary cilia act as microgravity sensors by depolymerizing microtubules to inhibit osteoblastic differentiation and mineralization. Bone. 2020;136:115346.
14. Al-Jallad HF, Myneni VD, Piercy-Kotb SA, Chabot N, Mulani A, Keillor JW, et al. Plasma membrane factor XIIIA transglutaminase activity regulates osteoblast matrix secretion and deposition by affecting microtubule dynamics. PLoS One. 2011;6:e15893.
15. Chen L, Shi K, Frary CE, Ditzel N, Hu H, Qiu W, et al. Inhibiting actin depolymerization enhances osteoblast differentiation and bone formation in human stromal stem cells. Stem Cell Res. 2015;15:281–289.
16. Higuchi C, Nakamura N, Yoshikawa H, Itoh K. Transient dynamic actin cytoskeletal change stimulates the osteoblastic differentiation. J Bone Min Metab. 2009;27:158–167.
17. Suzuki H, Tatei K, Ohshima N, Sato S, Izumi T. Regulation of MC3T3-E1 differentiation by actin cytoskeleton through lipid mediators reflecting the cell differentiation stage. Biochem Biophys Res Commun. 2019;514:393–400.
18. John AA, Prakash R, Kureel J, Singh D. Identification of novel microRNA inhibiting actin cytoskeletal rearrangement thereby suppressing osteoblast differentiation. J Mol Med (Berl). 2018;96:427–444.
19. Suozzi KC, Wu X, Fuchs E. Spectraplakins: master orchestrators of cytoskeletal dynamics. J Cell Biol. 2012;197:465–475.
20. Hu L, Xiao Y, Xiong Z, Zhao F, Yin C, Zhang Y, et al. MACF1, versatility in tissue-specific function and in human disease. Semin Cell Dev Biol. 2017;69:3–8.
21. Zhang J, Yue J, Wu X. Spectraplakin family proteins - cytoskeletal crosslinkers with versatile roles. J Cell Sci. 2017;130:2447–2457.
22. Oury J, Liu Y, Topf A, Todorovic S, Hoedt E, Preethish-Kumar V, et al. MACF1 links Rapsyn to microtubule- and actin-binding proteins to maintain neuromuscular synapses. J Cell Biol. 2019;218:1686–1705.
23. Wu X, Shen QT, Oristian DS, Lu CP, Zheng Q, Wang HW, et al. Skin stem cells orchestrate directional migration by regulating microtubule-ACF7 connections through GSK3beta. Cell. 2011;144:341–352.
24. Hu L, Su P, Li R, Yan K, Chen Z, Shang P, et al. Knockdown of microtubule actin crosslinking factor 1 inhibits cell proliferation in MC3T3-E1 osteoblastic cells. BMB Rep. 2015;48:583–588.
25. Ka M, Moffat JJ, Kim WY. MACF1 controls migration and positioning of cortical GABAergic interneurons in mice. Cereb Cortex. 2017;27:5525–5538.
26. Dobyns WB, Aldinger KA, Ishak GE, Mirzaa GM, Timms AE, Grout ME, et al. MACF1 mutations encoding highly conserved zinc-binding residues of the GAR domain cause defects in neuronal migration and axon guidance. Am J Hum Genet. 2018;103:1009–1021.
27. Yue J, Zhang Y, Liang WG, Gou X, Lee P, Liu H, et al. In vivo epidermal migration requires focal adhesion targeting of ACF7. Nat Commun. 2016;7:11692.
28. Qian AR, Hu LF, Gao X, Zhang W, Di SM, Tian ZC, et al. Large gradient high magnetic field affects the association of MACF1 with actin and microtubule cytoskeleton. Bioelectromagnetics. 2009;30:545–555.
29. Hu L, Su P, Yin C, Zhang Y, Li R, Yan K, et al. Microtubule actin crosslinking factor 1 promotes osteoblast differentiation by promoting beta-catenin/TCF1/Runx2 signaling axis. J Cell Physiol. 2018;233:1574–1584.
30. Zhang Y, Yin C, Hu L, Chen Z, Zhao F, Li D, et al. MACF1 overexpression by transfecting the 21-kbp large plasmid PEGFP-C1A-ACF7 promotes osteoblast differentiation and bone formation. Hum Gene Ther. 2018;29:259–270.
31. Qiu WX, Ma XL, Lin X, Zhao F, Li DJ, Chen ZH, et al. Deficiency of Macf1 in osterix expressing cells decreases bone formation by Bmp2/Smad/Runx2 pathway. J Cell Mol Med. 2020;24:317–327.
32. Livak KJ, Schmittgen TD. Analysis of relative gene expression data using real-time quantitative PCR and the $2^{-\Delta\Delta CT}$ Method. Methods. 2001;25:402–408.
33. Kim D, Pertea G, Trapnell C, Pimentel H, Kelley R, Salzberg SL. TopHat2: accurate alignment of transcriptomes in the presence of insertions, deletions and gene fusions. Genome Biol. 2013;14:R36.
34. Nueda MJ, Tarazona S, Conesa A. Next maSigPro: updating maSigPro bioconductor package for RNA-seq time series. Bioinformatics. 2014;30:2598–2602.
35. Robinson MD, McCarthy DJ, Smyth GK. edgeR: a Bioconductor package for differential expression analysis of digital gene expression data. Bioinformatics. 2010;26:139–140.
36. Langmead B, Salzberg SL. Fast gapped-read alignment with Bowtie 2. Nat Methods. 2012;9:357–359.
37. Landt SG, Marinov GK, Kundaje A, Kheradpour P, Pauli F, Batzoglou S, et al. ChIP-seq guidelines and practices of the ENCODE and modENCODE consortia. Genome Res. 2012;22:1813–1831.
38. Pillai S, Chellappan SP. ChIP on chip and ChIP-Seq assays: genome-wide analysis of transcription factor binding and histone modifications. Methods Mol Biol. 2015;1288:447–472.
39. Zhang Y, Liu T, Meyer CA, Eeckhoute J, Johnson DS, Bernstein BE, et al. Model-based analysis of ChIP-Seq (MACS). Genome Biol. 2008;9:R137.
40. Ramirez F, Ryan DP, Gruning B, Bhardwaj V, Kilpert F, Richter AS, et al. deepTools2: a next generation web server for deep-sequencing data analysis. Nucleic Acids Res. 2016;44:W160–165.
41. Heinz S, Benner C, Spann N, Bertolino E, Lin YC, Laslo P, et al. Simple combinations of lineage-determining transcription factors prime cis-regulatory elements required for macrophage and B cell identities. Mol Cell. 2010;38:576–589.
42. Komori T. Regulation of osteoblast differentiation by transcription factors. J Cell Biochem. 2006;99:1233–1239.
43. Li N, Felber K, Elks P, Croucher P, Roehl HH. Tracking gene expression during zebrafish osteoblast differentiation. Dev Dyn. 2009;238:459–466.
44. Lian N, Wang W, Li L, Elefteriou F, Yang X. Vimentin inhibits ATF4-mediated osteocalcin transcription and osteoblast differentiation. J Biol Chem. 2009;284:30518–30525.
45. Lian N, Lin T, Liu W, Wang W, Li L, Sun S, et al. Transforming growth factor β suppresses osteoblast differentiation via the vimentin activating transcription factor 4 (ATF4) axis. J Biol Chem. 2012;287:35975–35984.
46. Yu X, Shen G, Ren H, Zhang Z, Shang Q, Zhao W, et al. TGFβ-induced factor homeobox 2 blocks osteoblastic differentiation through targeting pSmad3/HDAC4/H4ac/Runx2 axis. J Cell Physiol. 2019;234:21284–21293.
47. Escobar-Aguirre M, Zhang H, Jamieson-Lucy A, Mullins MC. Microtubule-actin crosslinking factor 1 (Macf1) domain function in Balbiani body dissociation and nuclear positioning. PLoS Genet. 2017;13:e1006983.
48. Stein GS, Lian JB, van Wijnen AJ, Stein JL, Montecino M, Javed A, et al. Runx2 control of organization, assembly and activity of

the regulatory machinery for skeletal gene expression. Oncogene. 2004;23:4315–4329.
49. Nakashima K, Zhou X, Kunkel G, Zhang Z, Deng JM, Behringer RR, et al. The novel zinc finger-containing transcription factor osterix is required for osteoblast differentiation and bone formation. Cell. 2002;108:17–29.
50. Nishio Y, Dong Y, Paris M, O'Keefe RJ, Schwarz EM, Drissi H. Runx2-mediated regulation of the zinc finger Osterix/Sp7 gene. Gene. 2006;372:62–70.
51. Kawane T, Komori H, Liu W, Moriishi T, Miyazaki T, Mori M, et al. Dlx5 and mef2 regulate a novel runx2 enhancer for osteoblast-specific expression. J Bone Min Res. 2014;29:1960–1969.
52. Qin X, Jiang Q, Miyazaki T, Komori T. Runx2 regulates cranial suture closure by inducing hedgehog, Fgf, Wnt, and Pthlh signaling pathway gene expression in suture mesenchymal cells. Hum Mol Genet. 2019;28:896–911.
53. Gaur T, Lengner CJ, Hovhannisyan H, Bhat RA, Bodine PV, Komm BS, et al. Canonical WNT signaling promotes osteogenesis by directly stimulating Runx2 gene expression. J Biol Chem. 2005;280:33132–33140.
54. Chirackal Manavalan AP, Pilarova K, Kluge M, Bartholomeeusen K, Rajecky M, Oppelt J, et al. CDK12 controls G1/S progression by regulating RNAPII processivity at core DNA replication genes. EMBO Rep. 2019;20:e47592.
55. Ketley A, Wojciechowska M, Ghidelli-Disse S, Bamborough P, Ghosh TK, Morato ML, et al. CDK12 inhibition reduces abnormalities in cells from patients with myotonic dystrophy and in a mouse model. Sci Transl Med. 2020;12:eaaz2415.
56. Choi HJ, Jin S, Cho H, Won HY, An HW, Jeong GY, et al. CDK12 drives breast tumor initiation and trastuzumab resistance via WNT and IRS1-ErbB-PI3K signaling. EMBO Rep. 2019;20:e48058.
57. Lee AR, Li Y, Xie N, Gleave ME, Cox ME, Collins CC, et al. Alternative RNA splicing of the MEAF6 gene facilitates neuroendocrine prostate cancer progression. Oncotarget. 2017;8:27966–27975.
58. Rajgopal A, Young DW, Mujeeb KA, Stein JL, Lian JB, van Wijnen AJ, et al. Mitotic control of RUNX2 phosphorylation by both CDK1/cyclin B kinase and PP1/PP2A phosphatase in osteoblastic cells. J Cell Biochem. 2007;100:1509–1517.
59. Shen R, Wang X, Drissi H, Liu F, O'Keefe RJ, Chen D. Cyclin D1-cdk4 induce runx2 ubiquitination and degradation. J Biol Chem. 2006;281:16347–16353.
60. Micci F, Gorunova L, Gatius S, Matias-Guiu X, Davidson B, Heim S, et al. MEAF6/PHF1 is a recurrent gene fusion in endometrial stromal sarcoma. Cancer Lett. 2014;347:75–78.
61. Makise N, Sekimizu M, Kobayashi E, Yoshida H, Fukayama M, Kato T, et al. Low-grade endometrial stromal sarcoma with a novel MEAF6-SUZ12 fusion. Virchows Arch. 2019;475:527–531.
62. Sharma VP, Fenwick AL, Brockop MS, McGowan SJ, Goos JA, Hoogeboom AJ, et al. Mutations in TCF12, encoding a basic helix-loop-helix partner of TWIST1, are a frequent cause of coronal craniosynostosis. Nat Genet. 2013;45:304–307.
63. Trimarchi JM, Fairchild B, Wen J, Lees JA. The E2F6 transcription factor is a component of the mammalian Bmi1-containing polycomb complex. Proc Natl Acad Sci USA. 2001;98:1519–1524.
64. Xu X, Bieda M, Jin VX, Rabinovich A, Oberley MJ, Green R, et al. A comprehensive ChIP-chip analysis of E2F1, E2F4, and E2F6 in normal and tumor cells reveals interchangeable roles of E2F family members. Genome Res. 2007;17:1550–1561.
65. Yi S, Yu M, Yang S, Miron RJ, Zhang Y. Tcf12, a member of basic helix-loop-helix transcription factors, mediates bone marrow mesenchymal stem cell osteogenic differentiation in vitro and in vivo. Stem Cells. 2017;35:386–397.
66. Zou W, Greenblatt MB, Brady N, Lotinun S, Zhai B, de Rivera H, et al. The microtubule-associated protein DCAMKL1 regulates osteoblast function via repression of Runx2. J Exp Med. 2013;210:1793–1806.
67. Liu H, Zhang R, Ko SY, Oyajobi BO, Papasian CJ, Deng HW, et al. Microtubule assembly affects bone mass by regulating both osteoblast and osteoclast functions: stathmin deficiency produces an osteopenic phenotype in mice. J Bone Min Res. 2011;26:2052–2067.
68. Wang Y, Kakinuma N, Zhu Y, Kiyama R. Nucleo-cytoplasmic shuttling of human Kank protein accompanies intracellular translocation of beta-catenin. J Cell Sci. 2006;119:4002–4010.
69. Wilhelmsen K, Litjens SH, Kuikman I, Tshimbalanga N, Janssen H, van den Bout I, et al. Nesprin-3, a novel outer nuclear membrane protein, associates with the cytoskeletal linker protein plectin. J Cell Biol. 2005;171:799–810.
70. Ketema M, Sonnenberg A. Nesprin-3: a versatile connector between the nucleus and the cytoskeleton. Biochem Soc Trans. 2011;39:1719–1724.